

Article

Petrogenesis and Tectonic Setting of Ore-Associated Intrusive Rocks in the Baiyinnuoer Zn–Pb Deposit, Southern Great Xing’an Range (NE China): Constraints from Zircon U–Pb Dating, Geochemistry, and Sr–Nd–Pb Isotopes

Qing Zhao ^{1,*}, Rongge Xiao ¹, Dehui Zhang ¹, Jianping Wang ¹ , Yanfei Zhang ² and Panpan Li ¹

¹ School of Earth Sciences and Resources, China University of Geosciences, Beijing 100083, China; rgxiao@163.com (R.X.); zhdehui@cugb.edu.cn (D.Z.); jpwang@cugb.edu.cn (J.W.); mrlipanpan@163.com (P.L.)

² Liaoning Chemical Geology Exploration Institute, Jinzhou 121007, China; zhangyanfei_hgy@163.com

* Correspondence: qingzhao@cugb.edu.cn

Received: 2 December 2019; Accepted: 21 December 2019; Published: 24 December 2019



Abstract: The Baiyinnuoer skarn Zn–Pb deposit, located in the Southern Great Xing’an Range, Northeast China, is the largest Zn–Pb deposit of the northern China, with a total reserve of 32.74 Mt at average grades of 5.44% Zn and 2.02% Pb. The Zn–Pb ore bodies are hosted in the Lower Permian Huanggangliang Formation. The results of zircon U–Pb geochronology show that the ore-associated granodiorite porphyry, granodiorite, and diorite were emplaced at 248 ± 1.3 , 251 ± 1.8 , and 249 ± 1.4 Ma, respectively. The granodiorites and granodiorite porphyry have low P_2O_5 (0.13–0.23 wt %) and A/CNK (0.79–1.05) values, and their SiO_2 and P_2O_5 contents are negatively correlated, indicating I-type affinity. The positive $\epsilon Nd(t)$ values (+1.3 to +1.8) and young two-stage model ages (T_{DM2}) (880–916 Ma) of the Baiyinnuoer intrusive rocks suggest that they might have formed by the mixing of both mantle and crustal materials. The variations in the major elements, Rb, Sr, and Ba, and the negative Nb–Ta–Ti anomalies indicate that fractional crystallization might have occurred during magma ascent. In combination with the regional geology, the new geochronological, geochemical, and isotopic data reveal that the ore-associated intrusive rocks at Baiyinnuoer were formed in a post-collision setting in the Late Permian.

Keywords: Late Permian; I-type granitoid; skarn Zn–Pb deposit; Baiyinnuoer; Great Xing’an Range

1. Introduction

The Southern Great Xing’an Range (SGXR), Northeast (NE) China, located in the eastern part of the Central Asian Orogenic Belt (CAOB), is considered to be one of the most important metallogenic belts, hosting a number of skarn, porphyry, and magmatic–hydrothermal Pb–Zn–Ag–Cu–Mo polymetallic deposits [1–4] (Figure 1). Complex tectonic events have occurred in the region, including the closure of the Paleo-Asian Ocean in the Late Palaeozoic, the opening and closure of the Mongol–Okhotsk Ocean in the Mesozoic, and the subduction of the Paleo-Pacific Ocean in the Mesozoic [5–13].

The Baiyinnuoer skarn Zn–Pb deposit, located in the SGXR, is the largest Zn–Pb deposit in this region of northern China (Figure 1), with a total reserve of 32.74 Mt at average grades of 5.44% Zn, 2.02% Pb, and 31.4 g/t Ag [1,12,13]. Many recent investigations have focused on the geochronology, geochemistry, S–Pb isotopes, and fluid inclusions of the deposit [7,8,13–17]. Most scholars have regarded the Baiyinnuoer deposit as a skarn-type deposit, whereas Zeng et al. [7] considered it to

be a sedimentary exhalative deposit, on the basis of the S isotopic data of the sulfides. The age of the ore-associated intrusions and the related skarn-type Zn–Pb mineralization in the Baiyinnuoer deposit is still controversial. Shu et al. [1] reported the zircon U–Pb ages of the ore-associated granites and granodiorites (approximately 275 and 273 Ma, respectively) and suggested a Middle Permian age for the Zn–Pb mineralization. Yi et al. [16] estimated the age of the ore-related granodiorites as 242–245 Ma, proposing a Late Permian age for the Baiyinnuoer Zn–Pb mineralization. Jiang et al. [13] later identified skarn and vein types of mineralization, and suggested that the skarn mineralization was related to the granodiorites (Late Permian) and the vein-type mineralization was associated with the feldspar porphyries (Late Jurassic). Therefore, these key problems lie in the interpretation of the genetic relationships between the granitoids and the mineralization, and they require more precise geochemical, geochronological, and isotopic data.

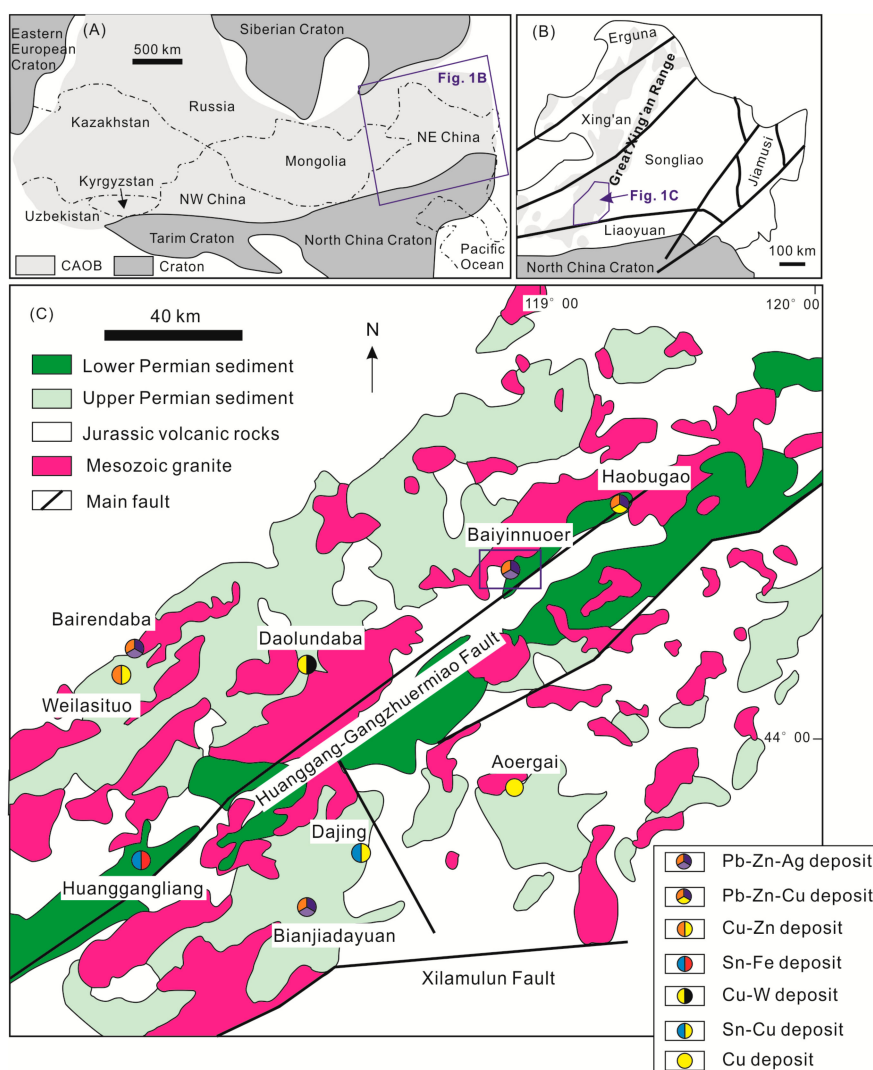


Figure 1. (A) Tectonic sketch map of the Central Asian Orogenic Belt (modified after [1,9,18]). (B) Simplified geological map of northeast China, showing the igneous rocks distributions within the Great Xing’an Range (modified after [1,6]). (C) Simplified geological map of the Southern Great Xing’an Range, showing the distributions of the main mineral deposits (modified after [1,3]).

In this study, we performed zircon U–Pb geochronological, whole rock geochemical, and Sr–Nd–Pb isotopic analyses of the ore-associated intrusive rocks in the Baiyinnuoer Zn–Pb deposit. These new data are used to better understand the ages, petrogenesis, and tectonic setting of the ore-associated intrusive rocks.

2. Geological Setting

Northeast China, which is located in the eastern part of the CAOB, is bounded by the North China Craton (NCC) to the south, and the Siberian Craton (SC) to the north [1,9,18–22] (Figure 1A). The Palaeozoic tectonic evolution of NE China includes the subduction of the Paleo-Asian Ocean and the amalgamation of multiple microcontinental blocks (e.g., the Jiamusi, Songliao, Xing'an, and Erguna blocks) [6,21–24] (Figure 1B). The Mesozoic tectonic evolution of this region is characterized by the Pacific plate tectonic regime in the east and the Mongol–Okhotsk plate tectonic regime in the northwest [6,21–24].

The SGXR, located in the western Songliao block [6,25,26] (Figure 1B), is characterized by widespread Late Paleozoic to Mesozoic volcanic-sedimentary successions (Figure 1C), and a number of world-class Pb–Zn–Ag–Cu–Mo polymetallic deposits are hosted in these successions (e.g., the Bairendaba, Huanggangliang, Bianjiadayuan, Dajing, and Haobugao deposits) [27–29]. The NE-trending Huanggang–Ganzhuermiao and EW-trending Xilamulun faults dominate this region and control the emplacement of the intrusions and the distributions of the polymetallic deposits [28–30] (Figure 1C). Moreover, intense magmatic events have been identified in this region, which has broadly distributed I- and A-type granitoids [5,6,21]. On the basis of a precise framework, these granitoids were considered to be emplaced in two geotectonic stages. The first group includes granodiorite, diorite, and tonalite with ages ranging from 321 to 237 Ma, which originated in the mantle and recycled ancient crustal materials, where the magmatism was associated with the closure of the Paleo-Asian Ocean, post-orogenic extension, and plate subduction [5,30–33]. The second group consists of monzogranite, syenogranite, and granodiorite with ages ranging from 150 to 131 Ma, which were derived from lower crustal materials, where the magmatism was related to plate subduction, lithospheric delamination, and extension [5,10,34,35].

According to the distributions of the polymetallic deposits, the SGXR metallogenic belt can be divided into three metallogenic sub-belts from west to east: the Xilinhot–Xilinguole Pb–Zn–Ag–Cu metallogenic sub-belt (e.g., the Bairendaba, Weilasituo, and Daolundaba deposits), the Huanggang–Ganzhuermiao Sn–Pb–Zn–Fe–Cu metallogenic sub-belt (e.g., the Huanggang, Dajing, Bianjiadayuan, and Haobugao deposits), and the Linxi–Lindong–Tianshan–Tuquan Cu–Mo metallogenic sub-belt (e.g., the Aoergai deposit) [5,13] (Figure 1C).

The Baiyinnuoer Zn–Pb deposit is a typical skarn Zn–Pb deposit in the SGXR, which belongs to the Huanggang–Ganzhuermiao Sn–Pb–Zn–Fe–Cu metallogenic sub-belt (Figure 1C). Exposed rocks include the Lower Permian Huanggangliang Formation and the Upper Jurassic Manketouebo Formation (Figure 2). The Huanggangliang Formation can be divided into three parts. The lower part is composed of sandy and argillaceous slates, and the middle part contains limestones, marbles, and skarns, with minor tuffs and andesites, and the upper part consists of slates with minor sandy and argillaceous slates (Figure 2). The Manketouebo Formation, unconformably overlaid on the Huanggangliang Formation, comprises tuffs and breccias. These units at Baiyinnuoer were intruded by Indosinian subvolcanic rocks (Late Permian–Middle Triassic), Yanshanian plutonic rocks (Late Jurassic–Early Cretaceous), and post-mineralization quartz porphyry dike (Early Cretaceous) [1] (Figure 2). Indosinian subvolcanic rocks consist of granodiorite, granodiorite porphyry, diorite, and syenite porphyry, which are genetically associated with the dominant skarn-type Zn–Pb mineralization [1]. Yanshanian plutonic rocks are composed of feldspar porphyry and feldspar-quartz porphyry, which are related to minor vein-type Zn–Pb mineralization [13]. Recent geochronological investigations indicated that the granodiorite, diorite, and feldspar porphyry were emplaced at approximately 244, 242, and 136 Ma, respectively [13,15,16].

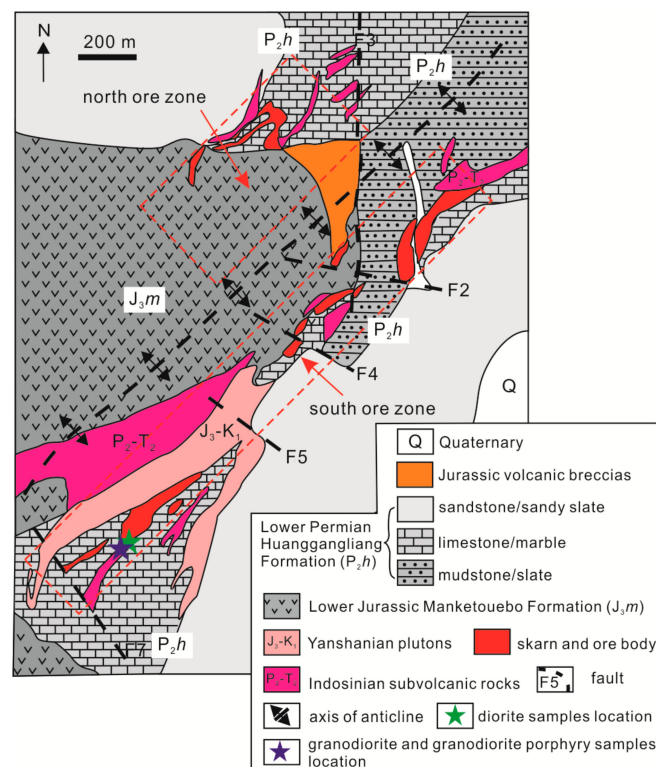


Figure 2. Geological map of the Baiyinnuoer Zn–Pb deposit, showing the north and south ore zones (modified after [1]).

The Baiyinnuoer Zn–Pb deposit is divided into the north and south ore zones (Figure 2). The south ore zone is approximately 2800 m long and 200–400 m wide, and it contains 55 ore bodies. The north ore zone is 1800 m long and 400–600 m wide, and it includes 108 ore bodies. The ore bodies contain galena and sphalerite with Pb and Zn grades of 2.02% and 5.44%, respectively [1,13]. Other ore minerals include chalcopyrite, pyrrhotite, and pyrite. The gangue minerals contain mainly chlorite, epidote, allanite, pyroxene, actinolite, garnet, feldspar, quartz, and calcite.

Detailed field observation around the south ore zone at Baiyinnuoer in this study revealed that the skarn-type Zn–Pb ore bodies occurred extensively, and these ore bodies developed along the contact zones between the Indosinian subvolcanic rocks and marbles.

3. Samples and Analytical Methods

3.1. Samples

In the Baiyinnuoer south ore zone, 11 samples, which belonged to the Indosinian subvolcanic group, were collected from underground tunnels, and the locations of the samples are shown in Figure 2. These studied ore-associated intrusions are composed of seven granodiorite samples, one granodiorite porphyry sample, and three diorite samples. The granodiorite is fine-grained and massive, and contains plagioclase (35%), K-feldspar (30%), quartz (15%), amphibole (15%), and minor biotite; all percentages are approximate (Figure 3A,B). The granodiorite porphyry shows porphyritic texture, and the phenocrysts contain amphibole (15%), plagioclase (15%), K-feldspar (5%), quartz (5%), and minor biotite, and the matrix consist of plagioclase (25%), K-feldspar (20%), quartz (10%), and amphibole (5%) (Figure 3C,D). The diorite consists of plagioclase (55%), amphibole (30%), and quartz (15%) (Figure 3E,F). Among these samples, one granodiorite sample, one granodiorite porphyry sample, and one diorite sample were analyzed by zircon U–Pb in situ LA-ICP-MS geochronology. One granodiorite porphyry sample and one diorite sample were analyzed for Sr–Nd–Pb isotopic analysis. Whole-rock geochemical analysis of all 11 samples was performed.

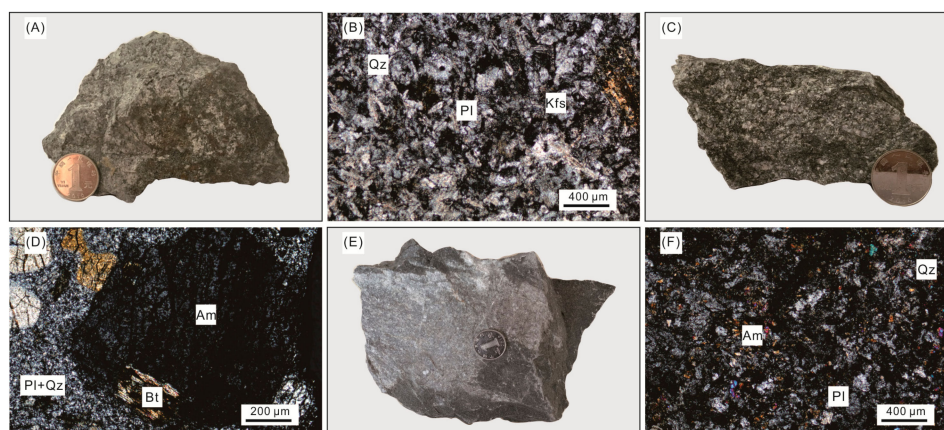


Figure 3. Photographs and photomicrographs of (A,B) granodiorite, (C,D) granodiorite porphyry, and (E,F) diorite in the Baiyinnuoer Zn–Pb deposit. Abbreviations: Qz—quartz, Pl—plagioclase, Kfs—K-feldspar, Am—amphibole, Bt—biotite.

3.2. Analytical Technique

3.2.1. Whole-Rock Geochemical Analysis

The major and trace element compositions were determined at the Institute of Geophysics and Geochemistry, Chinese Academy of Geological Sciences, Langfang, China. Each sample was crushed and powdered to less than 200 mesh in an agate mortar. The major elements were analyzed by X-ray fluorescence spectroscopy (Shimadzu WD-1800, Kyoto, Japan) using Chinese Standard GB/T14506.28–2010 [36]. Uncertainties were given at the 95% confidence level. The trace elements and rare earth elements (REE) were measured by ICP-MS using Chinese Standard Materials GSR-1, GSR-2, and GSR-3. Uncertainties were given at the 90% confidence level.

3.2.2. Whole-Rock Sr–Nd Isotopic Analysis

Whole-rock Sr–Nd isotopic analysis was performed at the Beijing Research Institute of Uranium Geology, China National Nuclear Corporation, Beijing, China. The sample was crushed and powdered to less than 200 mesh in an agate mortar. The Sr–Nd isotopes were identified by thermal ionization mass spectrometry (TIMS; Thermo-Finnigan Triton, Davis, CA, USA). The isotopic mass fractionation was corrected by normalizing to $^{88}\text{Sr}/^{86}\text{Sr} = 8.375209$ and $^{146}\text{Nd}/^{144}\text{Nd} = 0.7219$. In the analysis, measurement correction using the American Standard Materials NBS 987 yielded $^{87}\text{Sr}/^{86}\text{Sr} = 0.710250 \pm 0.000007$ (2σ) and $^{143}\text{Nd}/^{144}\text{Nd} = 0.512109 \pm 0.000003$ (2σ). The precision of the Sr–Nd isotopic analysis was better than 0.005%.

3.2.3. Whole-Rock Pb Isotopic Analysis

Whole-rock Pb isotopic analysis was performed at the Beijing Research Institute of Uranium Geology, China National Nuclear Corporation, Beijing, China. Each sample was crushed and powdered to less than 200 mesh in an agate mortar. A 0.2 g powder sample was digested by a mixed acid in a low-pressure airtight vessel. The aqueous solution was evaporated to dryness when it was fully dissolved after 24 h. After reacting with HCl to form chloride, the sample was separated by centrifugation. The Pb was dissociated using HCL, and the Pb isotopes were identified by TIMS (Isoprobe). The uncorrected results for NBS 981 were $^{206}\text{Pb}/^{204}\text{Pb} = 16.895 \pm 0.002$, $^{207}\text{Pb}/^{204}\text{Pb} = 15.437 \pm 0.002$, and $^{208}\text{Pb}/^{204}\text{Pb} = 36.537 \pm 0.004$.

3.2.4. Zircon U–Pb in Situ LA-ICP-MS Geochronology

Cathodoluminescence (CL) imaging of zircon grains was performed using an electron microscope at the Institute of Mineral Resources, China Academy of Geological Science, Beijing, China. Zircon U–Pb

geochronology was conducted using laser ablation inductively coupled plasma mass spectrometry (LA-ICP-MS) at the Testing Center of the Shandong Bureau of the China Metallurgical Geology Bureau, Jinan, China. A Coherent COMPex Pro ICP-MS instrument was used to acquire the ion signal intensities. Helium mixed with argon was used as a carrier gas. Each type of analysis incorporated a background acquisition followed by data acquisition from the sample. NIST 610 glass and Si were used as standards to perform the calibrations for the zircon analyses. Zircon 91,500 was used as an external standard for correcting U–Pb isotope fractionation effects. Concordia diagrams and weighted mean calculations were performed using Isoplot 3.0 [37]. Uncertainties were given at the 95% confidence level.

4. Results

4.1. Whole-Rock Geochemistry

The whole-rock major and trace element contents and REE data from seven granodiorite samples, one granodiorite porphyry sample, and three diorite samples are listed in Table S1. The granodiorite samples were slightly altered as the Loss on ignition (LOI) values ranging from 0.54 to 1.35 wt %. One granodiorite porphyry sample (BY02) and two diorite samples (BY09 and BY11) might experience modest alteration, leading their LOI values to be 3.24, 4.60, and 3.00 wt %, respectively (Table S1).

The granodiorites and granodiorite porphyry in the Baiyinnuoer deposit have high SiO_2 contents of 65.05–68.25 wt % (Figure 4A), with an average value of 67.38 wt %. The Al_2O_3 , Na_2O , K_2O , FeO_t , MgO , and CaO contents are 13.11–14.30, 2.09–4.42, 2.40–5.42, 1.66–3.70, 1.21–2.15, and 1.93–4.39 wt %, respectively. They also have low TiO_2 (0.37–0.55 wt %) and P_2O_5 (0.13–0.23 wt %) contents. The Mg# values of the granodiorites (porphyries) range from 43 to 65. In the K_2O versus SiO_2 diagram (Figure 4A), most samples plot into the high-K calc-alkaline field. The granodiorites and granodiorite porphyry are metaluminous with A/CNK (molar $\text{Al}_2\text{O}_3/\text{CaO} + \text{Na}_2\text{O} + \text{K}_2\text{O}$) values of 0.79–1.05 and A/NK (molar $\text{Al}_2\text{O}_3/\text{Na}_2\text{O} + \text{K}_2\text{O}$) values of 1.21–1.69 (Figure 4B). Moreover, the granodiorites and granodiorite porphyry have REE contents of 97.03–144.36 ppm and are enriched in light rare earth element (LREE), with $(\text{La}/\text{Yb})_N$ ratios of 7.60–13.27. The granodiorites and granodiorite porphyry also show slight Eu anomalies ($\delta\text{Eu} = 0.54\text{--}0.82$; $\delta\text{Eu} = 2 \times (\text{Eu}/0.0735)/((\text{Sm}/0.195) + (\text{Gd}/0.259))$) and negligible Ce anomalies ($\delta\text{Ce} = 0.86\text{--}1.06$; $\delta\text{Ce} = 2 \times (\text{Ce}/0.808)/((\text{La}/0.310) + (\text{Pr}/0.122))$) (Figure 5A). As shown in the primitive-mantle-normalized trace element spider diagram (Figure 5B), the granodiorites and granodiorite porphyry are enriched in Rb, Th, and U, and depleted in Nb, Ta, and Ti.

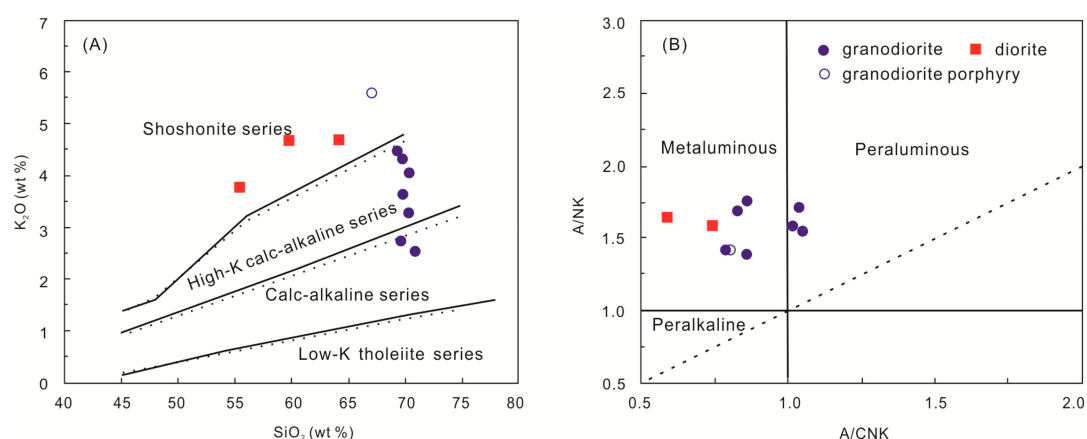


Figure 4. Geochemical classification diagrams of the Baiyinnuoer intrusive rocks. (A) K_2O versus SiO_2 (modified after [38]). (B) A/NK versus A/CNK (modified after [39,40]).

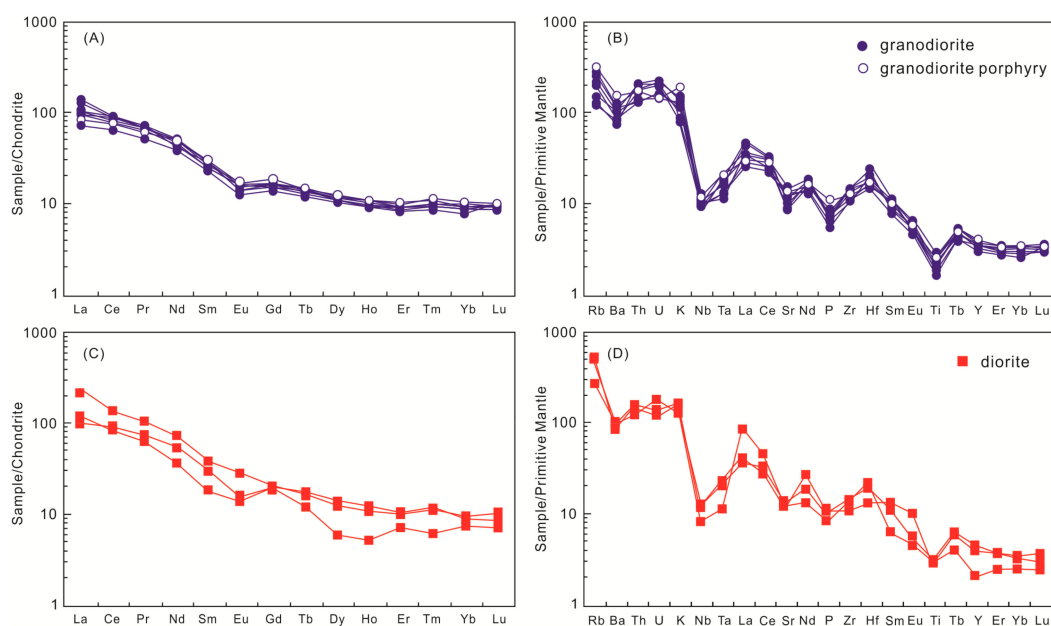


Figure 5. Chondrite-normalized rare earth element (REE) patterns and primitive-mantle-normalized multi-element spidergrams for the granodiorite and granodiorite porphyry (A,B) and the diorite (C,D) in the Baiyinnuoer Zn–Pb deposit. Chondrite-normalized and primitive-mantle-normalized values are from [41].

With respect to the diorite samples, the SiO_2 contents range from 53.53 to 60.14 wt %, with an average of 57.16 wt %. The diorites have high FeO_t (5.04–6.82 wt %), TiO_2 (0.59–0.64 wt %), MgO (3.02–4.06 wt %), and CaO (4.64–11.69 wt %) contents, and low Al_2O_3 (12.71–14.07 wt %) and Na_2O (2.06–2.56 wt %) contents. The diorites yield $\text{Mg}\#$ values of 50–55. In the K_2O versus SiO_2 diagram, the diorites are all plotted in the shoshonitic field (Figure 4A). The diorites are metaluminous, with A/CNK values of 0.44–0.74 (Figure 4B). Moreover, the diorites have REE contents of 113.7–199.0 ppm and $(\text{La}/\text{Yb})_N$ ratios of 10.55–22.23, indicating a distinct fractionation between heavy rare earth element (HREE) and LREE (Figure 5C). The diorites show negligible Eu and Ce anomalies ($\delta\text{Eu} = 0.60\text{--}0.98$; $\delta\text{Ce} = 0.76\text{--}0.99$) (Figure 5C) and negative Nb–Ta–Ti anomalies (Figure 5D).

4.2. Whole-Rock Sr–Nd Isotopic Results

The Sr–Nd isotopic compositions of one granodiorite sample and one diorite sample, from the Baiyinnuoer deposit are listed in Table S2 and plotted in Figure 6. The granodiorite sample BY08 has an initial $^{87}\text{Sr}/^{86}\text{Sr}$ ratio of 0.7054, an $\varepsilon\text{Nd}(t)$ value of +1.0 ($t = 251$ Ma), and a $T_{\text{DM}2}$ value of 937 Ma. The diorite sample BY10 has an initial $^{87}\text{Sr}/^{86}\text{Sr}$ ratio of 0.7044, an $\varepsilon\text{Nd}(t)$ value of +1.8 ($t = 249$ Ma), and a $T_{\text{DM}2}$ value of 880 Ma.

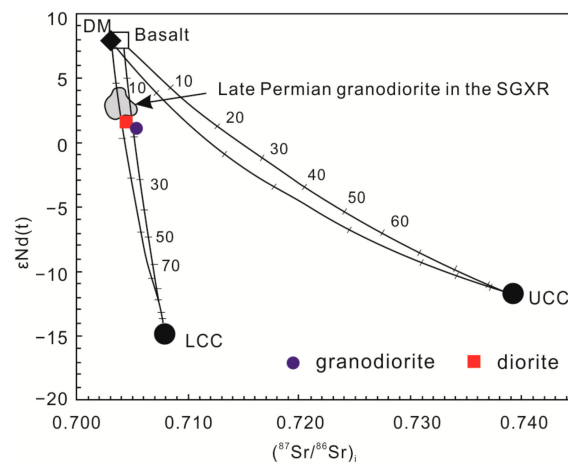


Figure 6. $\epsilon\text{Nd}(t)$ versus $(^{87}\text{Sr}/^{86}\text{Sr})_i$ for the Baiyinnuoer intrusive rocks, showing the mixing proportions of two end members: depleted mantle or juvenile components and crustal materials (modified after [42]). Abbreviations: DM—upper mantle peridotite; B—basalt; LCC—lower continental crust; UCC—upper continental crust. Data are from Jiang et al. [13] and this study.

4.3. Whole-Rock Pb Isotopic Results

The Pb isotopic compositions of one granodiorite sample and one diorite sample from the Baiyinnuoer deposit are listed in Table S3 and plotted in Figure 7. The granodiorite sample BY08 shows $^{208}\text{Pb}/^{204}\text{Pb}$, $^{207}\text{Pb}/^{204}\text{Pb}$, and $^{206}\text{Pb}/^{204}\text{Pb}$ ratios of 38.56, 15.557, and 18.712, respectively. The diorite sample BY10 has $^{208}\text{Pb}/^{204}\text{Pb}$, $^{207}\text{Pb}/^{204}\text{Pb}$, and $^{206}\text{Pb}/^{204}\text{Pb}$ values of 38.203, 15.557, and 18.334, respectively.

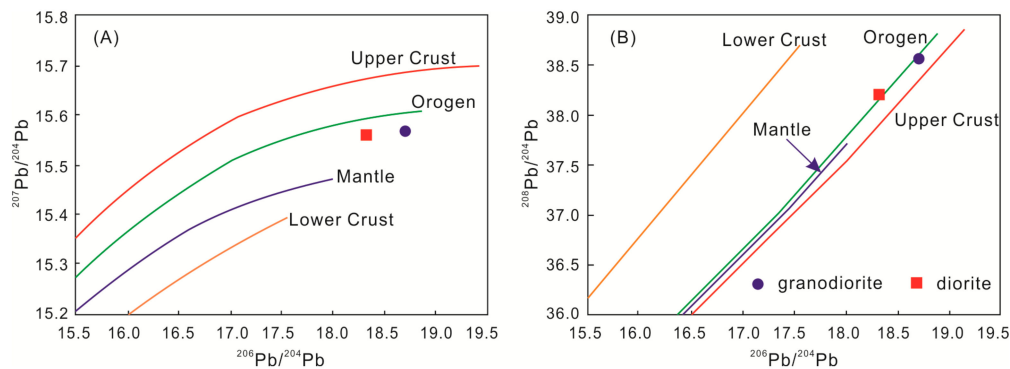


Figure 7. Plot of Pb isotopic data for the Baiyinnuoer intrusive rocks. (A) $^{207}\text{Pb}/^{204}\text{Pb}$ versus $^{206}\text{Pb}/^{204}\text{Pb}$. (B) $^{208}\text{Pb}/^{204}\text{Pb}$ versus $^{206}\text{Pb}/^{204}\text{Pb}$ (modified after [43]).

4.4. Zircon U–Pb Geochronology

The results of zircon U–Pb dating of one granodiorite porphyry sample, one granodiorite sample, and one diorite sample in the Baiyinnuoer deposit are presented in Table S4, and the representative CL images of zircon grains are shown in Figure 8, and the concordia diagrams of the zircon U–Pb isotopic data are illustrated in Figure 9.

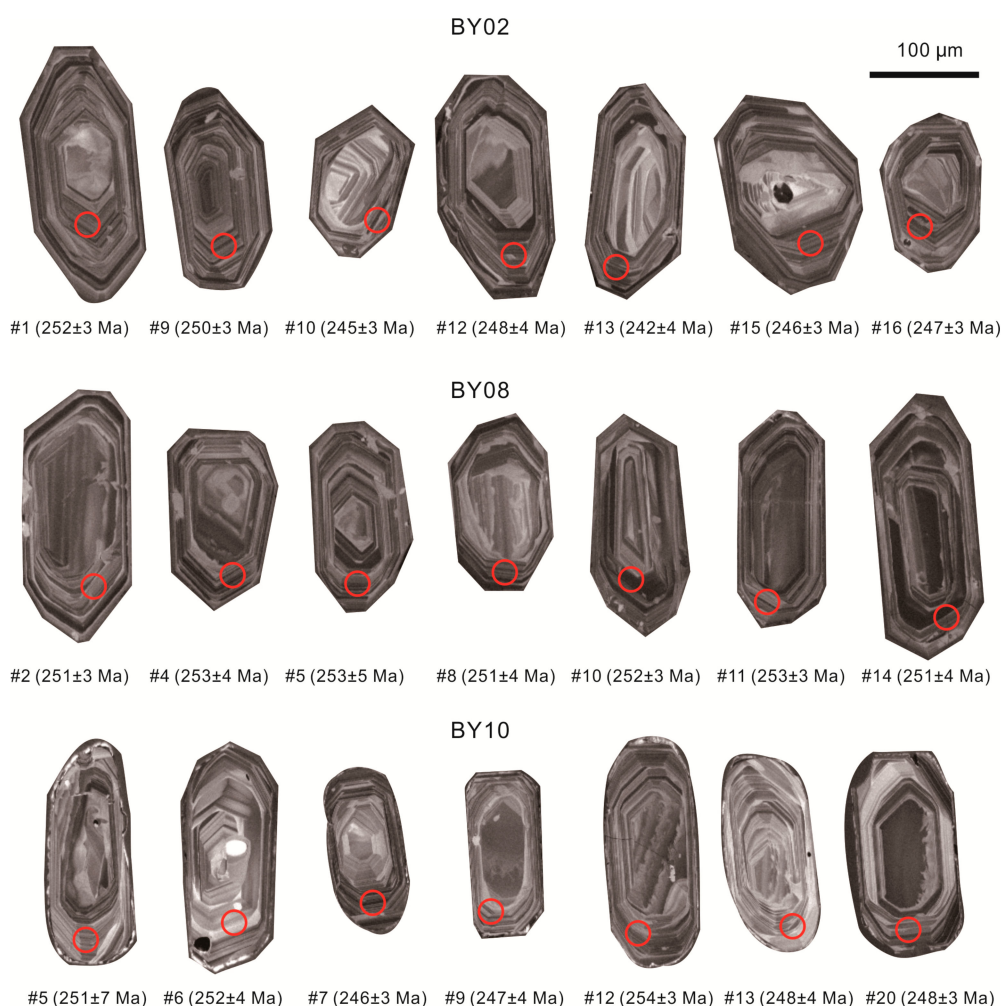


Figure 8. Representative cathodoluminescence images of zircon grains from granodiorite porphyry (BY02), granodiorite (BY08), and diorite (BY10) samples from the Baiyinnuoer Zn–Pb deposit.

Zircon grains from the granodiorite porphyry sample BY02 are euhedral–subhedral prismatic grains with oscillatory zoning texture (Figure 8). They are 120–260 µm in size, and their length/width ratios are 2:1–3:1 (Figure 8). Twenty-two zircon grains were analyzed, and their Th and U contents are 127.4–614.4 and 404.6–1517.9 ppm (Table S4), respectively. The Th/U ratios range from 0.25 to 0.46 (Table S4), indicating a magmatic origin [44]. These zircons show $^{206}\text{Pb}/^{238}\text{U}$ ages of 242–253 Ma (Table S4) and yield a mean age of 248 ± 1.3 Ma (MSWD = 0.61, $n = 22$) (Figure 9A,B), which could represent the crystallization age of the granodiorite porphyry.

Zircon grains from the granodiorite sample BY08 are euhedral–subhedral prismatic grains with an oscillatory zoning texture (Figure 8). The sizes of these grains are 160–260 µm, and their length/width ratios are 2:1–3:1 (Figure 8). Fourteen zircon grains were analyzed, and their Th and U contents are 74.4–506.5 and 289.5–931.1 ppm (Table S4), respectively. The Th/U ratios range from 0.31 to 0.54 (Table S4), indicating a magmatic origin [44]. These zircons show $^{206}\text{Pb}/^{238}\text{U}$ ages of 247–253 Ma (Table S4) and yield a mean age of 251 ± 1.8 Ma (MSWD = 0.36, $n = 14$) (Figure 9C,D), which could represent the crystallization age of the granodiorite.

The zircons from the diorite sample BY10 present as euhedral–subhedral prismatic grains, with lengths of 160–300 µm and length/width ratios of 2:1–3:1 (Figure 8). Twenty-three zircon grains were analyzed, and most of them exhibited oscillatory zoning texture (Figure 8). These grains have U = 315.3–1243.8 ppm, Th = 117.3–912.0 ppm, and Th/U = 0.29–0.73 (Table S4), indicating a magmatic origin [44]. Twenty-three analyzed spots show $^{206}\text{Pb}/^{238}\text{U}$ ages ranging from 245 to 254 Ma (Table S4)

and yield a mean age of 249 ± 1.4 Ma (MSWD = 0.74, $n = 23$) (Figure 9E,F), which could represent the magmatic crystallization age of the diorite.

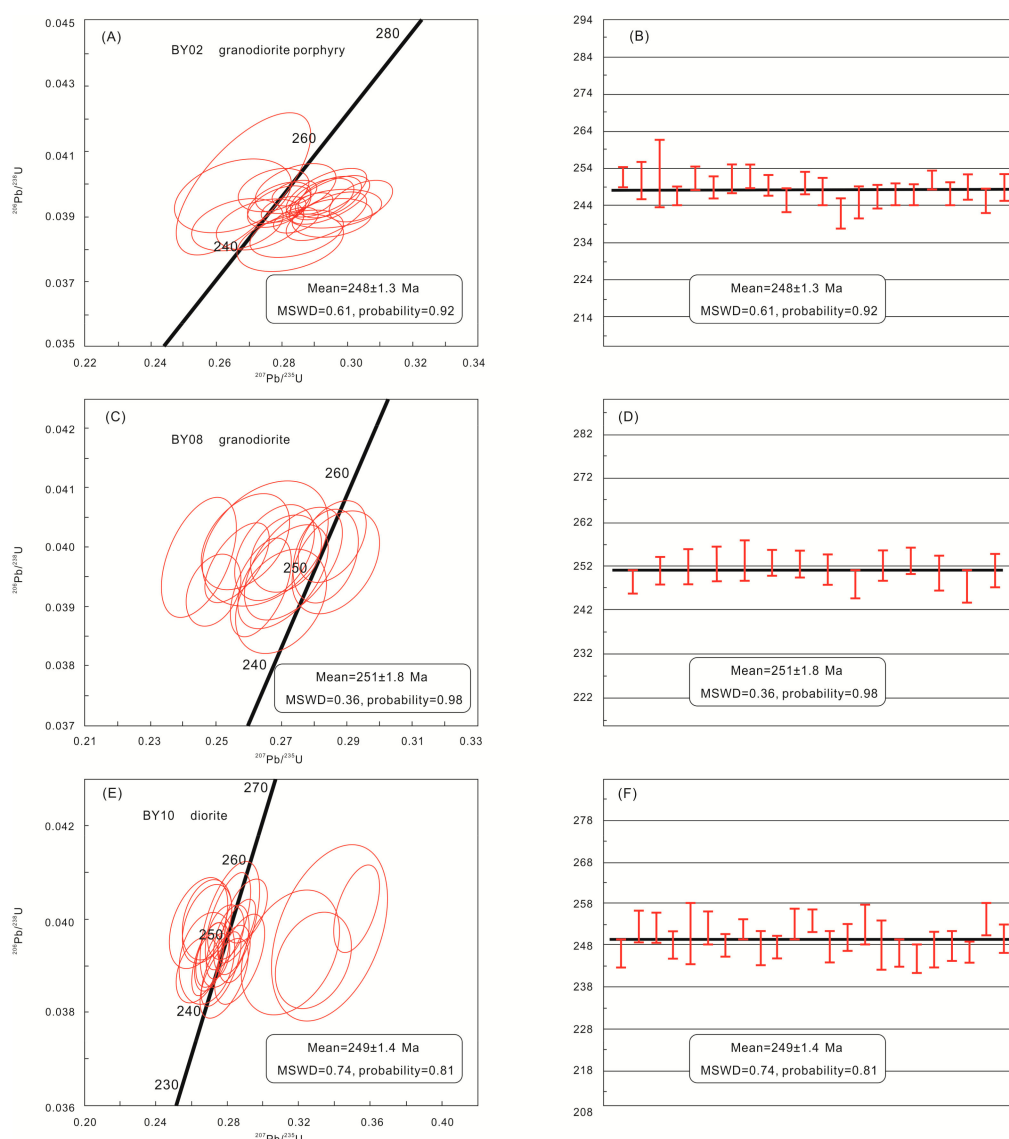


Figure 9. Concordia diagrams of zircon U–Pb isotopic data from the granodiorite porphyry sample BY02 (A,B), granodiorite sample BY08 (C,D), and diorite sample BY10 (E,F) in the Baiyinnuoer Zn–Pb deposit.

5. Discussion

5.1. Age of Magmatism

Several geochronological studies on Indosinian subvolcanic rocks at Baiyinnuoer have been undertaken to determine the precise age of magmatism. Yang et al. [17] reported that the granodiorites were emplaced at approximately 253 Ma. Jiang et al. [13] suggested that the crystallization age of the granodiorite was approximately 244 Ma. However, Shu et al. [1] reported that the granodiorites and granites were emplaced at approximately 273 and 275 Ma, respectively.

In this study, zircon grains from the granodiorite porphyry, granodiorite, and diorite commonly are euhedral–subhedral prismatic grains, and exhibit oscillatory zoning texture (Figure 8). These features, together with the high Th/U ratios, indicate a magmatic origin [44]. The zircons from the granodiorite porphyry sample BY02, the granodiorite sample BY08, and the diorite sample BY10 yield mean $^{206}\text{Pb}/^{238}\text{U}$ ages of 248 ± 1.3 , 251 ± 1.8 , 249 ± 1.4 Ma, respectively. Accordingly, Indosinian

subvolcanic rocks were emplaced in the Late Permian and we can constrain the age of magmatism at Baiyinnuoer to 251–248 Ma.

In the Great Xing'an Range, ore-associated Indosinian magmatic rocks occur extensively. The zircon U–Pb geochronology in the Aoergai copper deposit showed that the ore-related granodiorites were emplaced at approximately 245 Ma [45]. Ore-related granite yielded a $^{206}\text{Pb}/^{238}\text{U}$ age of approximately 243 Ma, which occurred widespread in the Badaguan Cu–Mo deposit [46]. The ages of mineralization of these deposits are similar to those of Indosinian magmatic rocks within the Great Xing'an Range. Further exploration in the Great Xing'an Range, therefore, might focus on the Late Permian–Early Triassic magmatism.

5.2. Source and Petrogenesis of the Magma

5.2.1. Granodiorite and Granodiorite Porphyry

Accurately recognizing the genetic type of the granitoids is important for understanding the source and petrogenesis of the magma and determining the tectonic setting [47]. The granitoids are classified as A-, I-, M-, and S-type [48–50]. In general, A-type granitoids have high ($\text{Na}_2\text{O} + \text{K}_2\text{O}$) and high field strength elements (HFSEs) contents and might be generated in extensional settings [51]. By contrast, I-type granitoids have low P_2O_5 contents and high Th and Y values, and could have been derived from igneous rocks, whereas S-type granitoids are considered to be derived from metasedimentary rocks [52,53].

In the Baiyinnuoer Zn–Pb deposit, the high-K calc-alkaline granodiorites and granodiorite porphyry have high SiO_2 contents (65.05–68.25 wt %) and low FeO_t/MgO ratios (0.94–2.33). They are metaluminous, with A/CNK values of 0.79–1.05, suggesting an important criterion for I-type granitoids [52,53]. In the discrimination diagrams, the granodiorites and granodiorite porphyry all plot into the unfractionated I-, M-, and S-type granitoids fields (Figure 10A,B). Moreover, all the granodiorites and granodiorite porphyry have low P_2O_5 contents (0.13–0.23 wt %) and show negative correlations between SiO_2 and P_2O_5 (Figure 10C), indicating I-type affinity. Accordingly, we consider that the granodiorites and granodiorite porphyry in the Baiyinnuoer Zn–Pb deposit are metaluminous, high-K calc-alkaline I-type granitoids.

The petrogenesis of I-type granitoids remains controversial. Previous petrological investigations have demonstrated that I-type granitoids could have been formed by the partial melting of igneous rocks in the lower crust [54], the mixing of mantle-derived mafic magma and crust-derived felsic magma [55], or by the fractional crystallization of mantle-derived mafic magma [56,57]. The I-type granodiorites and granodiorite porphyry in the Baiyinnuoer deposit show a small positive correlation between La/Sm and La (Figure 10D), possibly suggesting partial melting rather than fractional crystallization. Therefore, a model of fractional crystallization of mantle-derived mafic magma was precluded. It is widely acknowledged that the magmas, which were derived from the partial melting of lower crustal mafic rocks, generally have low Mg# values (<40) and MgO contents [58]. The I-type granodiorites and granodiorite porphyry in the Baiyinnuoer deposit have higher Mg# (43–65) and MgO (1.36–2.15 wt %) values than typical crust-derived melts [59,60], suggesting that mantle components were involved in their genesis. Furthermore, the granodiorites and granodiorite porphyry have relatively low Nb/Ta ratios (8.48–15.01), which are lower than that of the primitive mantle (17) [61] but close to that of the crust (11) [61], suggesting the involvement of crustal materials. The low Zr/Hf (20.30–29.89) and Nb/La ratios (0.19–0.43) also indicate that crustal components were added to the magma source [61]. Accordingly, we consider that the I-type granodiorites and granodiorite porphyry in the Baiyinnuoer deposit resulted from mixing of mantle-derived and crust-derived magmas.

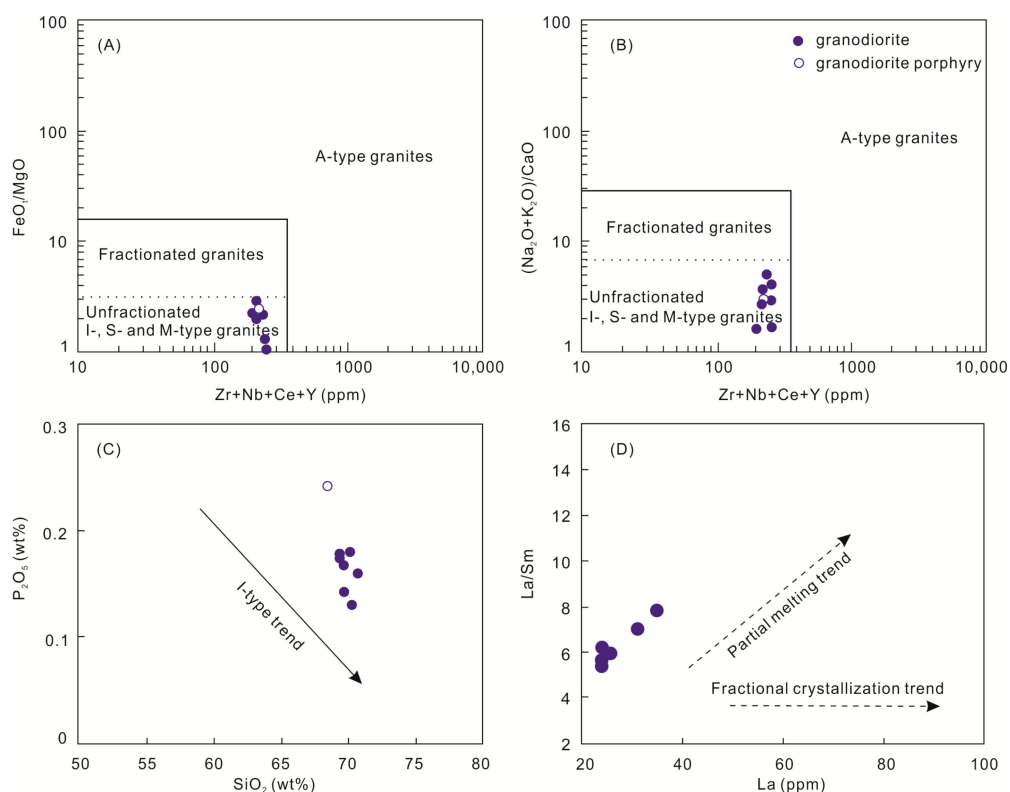


Figure 10. Discrimination diagrams of the Baiyinnuoer granodiorites and granodiorite porphyry (modified after [51]). (A) FeO_t/MgO versus $\text{Zr} + \text{Nb} + \text{Ce} + \text{Y}$. (B) $(\text{Na}_2\text{O} + \text{K}_2\text{O})/\text{CaO}$ versus $\text{Zr} + \text{Nb} + \text{Ce} + \text{Y}$. (C) P_2O_5 versus SiO_2 . (D) La/Sm versus La .

The Sr–Nd isotopic data might provide more evidence regarding their genesis. The granodiorite sample BY08 has a positive $\epsilon\text{Nd}(t)$ value (+1.3) and young $T_{\text{DM}2}$ age (916 Ma), indicating a juvenile source. Wu et al. [42] proposed a two-component mixing model to constrain the proportions of ancient and juvenile materials. According to this model, as shown in Figure 6, the Baiyinnuoer granodiorite could have been generated from a mixture of approximately 20% mantle-derived components and 80% lower continental crustal materials. Accordingly, the parent magmas of the Baiyinnuoer granodiorites and granodiorite porphyry were originated in a mixture of mantle-derived components and lower continental crustal materials.

Moreover, the pronounced negative Eu, Nb, Ta, and Ti anomalies indicate that fractional crystallization might have occurred during magma ascent. The negative Eu anomalies might result from the fractionation of plagioclase and/or K-feldspar in the magma chamber. As shown in Figure 11A,B, the fractionating phases of amphibole and biotite might be included. The fractionation of Ti-bearing phases (e.g., ilmenite and titanite) and apatite might result in negative Nb–Ta–P–Ti anomalies (Figure 11C,D).

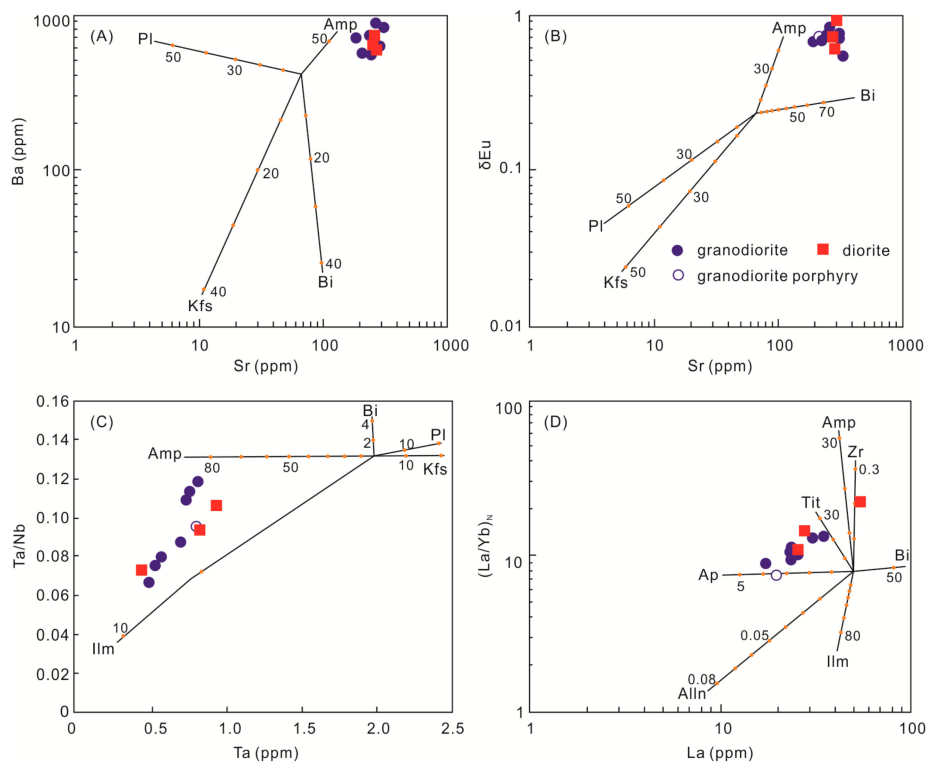


Figure 11. Discrimination diagrams of the Baiyinnuoer intrusive rocks (modified after [62]). (A) Ba versus Sr. (B) Eu versus Sr. (C) Ta/Nb versus Ta. (D) $(La/Yb)_N$ versus La.

5.2.2. Diorite

The diorites show metaluminous characteristics (Figure 4A,B), together with the fractionated REE patterns and Nb–Ta–Ti anomalies (Figure 5C,D), suggesting a close resemblance to typical arc-related rocks [58]. The diorites have low SiO_2 contents (53.53–60.14 wt %) and high MgO (3.02–4.06 wt %), Cr (76.9–121.3 ppm), Co (12.14–15.86 ppm), Ni (19.36–31.78 ppm), and Mg# (50–55) values, indicating that their parental magmas could not have been produced by the partial melting of crustal rocks, and thus a mantle source is favored [63]. The Nb/Ta (9.50–13.77), Zr/Hf (25.72–27.37), Nb/La (0.11–0.36), and Nb/U (1.67–3.58) ratios suggest the involvement of crustal components in their genesis [61]. Furthermore, the geochemical characteristics of the diorites are similar to those of the granodiorites and granodiorite porphyry in our study (Figure 5), possibly indicating that they have the same magma source. The diorite sample BY10 has a positive $\epsilon Nd(t)$ value (+1.8) and a young T_{DM2} age (880 Ma), indicating a juvenile magma source. As shown in Figure 6, the diorite could have been generated from a mixture of approximately 20% mantle-derived components and 80% lower continental crustal materials [42]. The fractionation of amphibole, biotite, ilmenite, titanite, and zircon might have occurred during magma ascent (Figure 11A,D).

Accordingly, we consider that the 251–248 Ma intrusive rocks in the Baiyinnuoer deposit could have been derived from mixing of mantle-derived and crust-derived juvenile magmas, and little ancient crustal material was added to their genesis. The fractional crystallization of plagioclase and/or K-feldspar, amphibole, biotite, ilmenite, titanite, and apatite might have occurred in these intrusive rocks during magma ascent.

5.3. Tectonic Implications

Recent studies have shown that the Paleo-Asian Ocean developed mainly from the Mesoproterozoic, which was located in the CAOB between the NCC and SC [6,64]. However, controversy remains regarding where and when the Paleo-Asian Ocean closed. Several researchers have suggested that the Hegenshan–Heihe suture (between the Xing’an and Songliao blocks) could

represent the final closure of the ocean during the Late Devonian–Early Carboniferous [22,65,66], as evidenced by the palaeomagnetic data from the northern NCC. Nevertheless, most scholars consider that the Solonker–Xra Moron–Changchun suture (between the Songliao and Liaoyuan blocks) might represent the final collision zone and they suggested that the suturing might take place at 250 Ma [6,9,10,22,67–70], and this hypothesis is supported by the arc-related volcanic rocks and palaeontological evidence (e.g., fossils). Jian et al. [71] summarized the published zircon U–Pb age data of the ophiolite in the Solonker mélangé and constrained the age of post-collisional magmatism in this region at 255–248 Ma, suggesting that this magmatic episode might follow the complete closure of Paleo-Asian Ocean in the Late Permian. In this study, our new data from the Baiyinnuoer intrusive rocks could provide more clues for deciphering the geological setting of the SGXR during the Late Permian.

The I-type granodiorites and granodiorite porphyry are enriched in LREE and HFSEs, and show typical calc-alkaline characteristics with negative Nb–Ta–Ti anomalies (Figures 4 and 5), indicating an arc-related setting. The Pb isotopic data of the Baiyinnuoer intrusive rocks suggest an orogenic setting during the Late Permian (Figure 7). Moreover, the tectonic discrimination diagrams show that the granodiorites and granodiorite porphyry all plot into the post-orogenic granite field (Figure 12), indicating that the Baiyinnuoer granodiorites and granodiorite porphyry were generated in a post-collision setting in the Late Permian. Accordingly, considering the regional geology, we propose a post-collision setting for the emplacement of the granodiorites and granodiorite porphyry in the Baiyinnuoer Zn–Pb deposit. In light of the new geochemical, geochronological, and isotopic data, the intrusive rocks were considered to be formed in a post-collision setting in the Late Permian (251–248 Ma), and could have been derived from the mixing of mantle-derived components and lower continental crustal materials, with subsequent fractional crystallization.

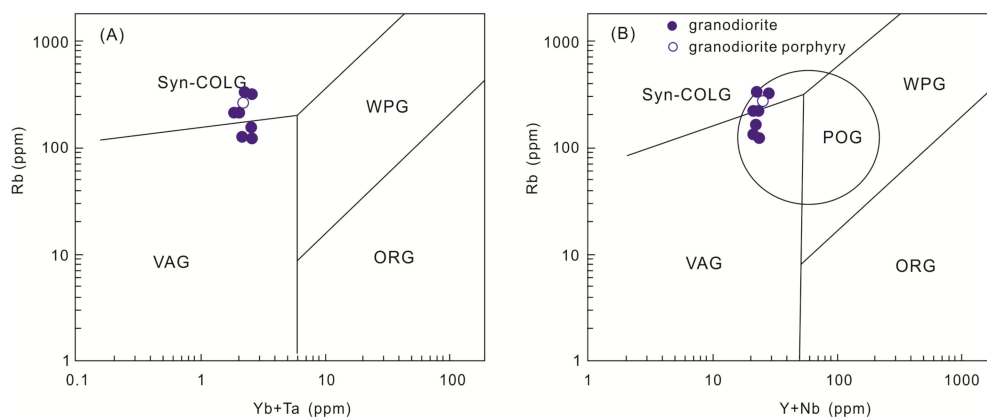


Figure 12. Discrimination diagrams of the Baiyinnuoer intrusive rocks. (A) Rb versus Yb + Ta. (B) Rb versus Y + Nb (modified after [72]). Abbreviations: WPG—within plate granites; VAG—volcanic arc granites; Syn-COLG—syn-collision granites; ORG—ocean ridge granites; POG—post-collision granites.

6. Conclusions

Geochronological data confirm that the Baiyinnuoer granodiorites, granodiorite porphyry, and diorites were formed in the Late Permian (251–248 Ma). The granodiorites and granodiorite porphyry are high-K calc-alkaline and show typical features similar to those of I-type granitoids. These intrusive rocks were likely derived from the mixing of mantle-derived components and lower continental crustal materials. The geochemical and isotopic results reveal a post-collision setting for the emplacement of these intrusive rocks at Baiyinnuoer. Therefore, the SGXR might experience the closure of the Paleo-Asian Ocean in the Late Permian.

Supplementary Materials: The following are available online at <http://www.mdpi.com/2075-163X/10/1/19/s1>, Table S1: Whole-rock geochemical data from the intrusive rocks in the Baiyinnuoer Zn–Pb deposit; Table S2: Sr–Nd isotopic data from the intrusive rocks in the Baiyinnuoer Zn–Pb deposit; Table S3: Pb isotopic data from

the intrusive rocks in the Baiyinnuoer Zn–Pb deposit; Table S4: LA-ICP-MS zircon U–Pb isotopic data from the intrusive rocks in the Baiyinnuoer Zn–Pb deposit.

Author Contributions: Q.Z. wrote the paper; R.X., D.Z., and J.W. designed the experiments; Y.Z. and P.L. took part in the field investigation. All authors have read and agreed to the published version of the manuscript.

Funding: This study was funded by the National Natural Science Foundation of China (No. 41730426, 41272106, 41030423).

Acknowledgments: The authors thank Li Fengchun and Xu Shuang for the zircon U–Pb dating. The authors are grateful to the critical and thoughtful comments from the editors and the anonymous reviewers which profoundly enhanced the quality of this manuscript.

Conflicts of Interest: The authors declare no conflict of interest.

References

- Shu, Q.; Lai, Y.; Sun, Y.; Wang, C.; Meng, S. Ore genesis and hydrothermal evolution of the Baiyinnuoer zinc–lead skarn deposit, Northeast China: Evidence from isotopes (S, Pb) and fluid inclusions. *Econ. Geol.* **2013**, *108*, 835–860. [[CrossRef](#)]
- Shu, Q.; Lai, Y.; Wang, C.; Xu, J.; Sun, Y. Geochronology, geochemistry and Sr–Nd–Hf isotopes of the Haisugou porphyry Mo deposit, northeast China, and their geological significance. *J. Asian Earth Sci.* **2014**, *79*, 777–791. [[CrossRef](#)]
- Zhai, D.; Liu, J.; Zhang, H.; Yao, M.; Wang, J.; Yang, Y. S–Pb isotopic geochemistry, U–Pb and Re–Os geochronology of the Huanggangliang Fe–Sn deposit, Inner Mongolia, NE China. *Ore Geol. Rev.* **2014**, *59*, 109–122. [[CrossRef](#)]
- Zhai, D.; Liu, J.; Zhang, H.; Tombros, S.; Zhang, A. A magmatic-hydrothermal origin for Ag–Pb–Zn vein formation at the Bianjiadayuan deposit, inner Mongolia, NE China: Evidences from fluid inclusion, stable (C–H–O) and noble gas isotope studies. *Ore Geol. Rev.* **2018**, *101*, 1–16. [[CrossRef](#)]
- Wu, F.-Y.; Lin, J.-Q.; Wilde, S.A.; Zhang, X.; Yang, J.-H. Nature and significance of the Early Cretaceous giant igneous event in eastern China. *Earth Planet. Sci. Lett.* **2005**, *233*, 103–119. [[CrossRef](#)]
- Wu, F.-Y.; Sun, D.-Y.; Ge, W.-C.; Zhang, Y.-B.; Grant, M.L.; Wilde, S.A.; Jahn, B.-M. Geochronology of the Phanerozoic granitoids in northeastern China. *J. Asian Earth Sci.* **2011**, *41*, 1–30. [[CrossRef](#)]
- Zeng, Q.D.; Liu, J.M.; Jia, C.S.; Wan, Z.M.; Yu, C.M.; Ye, J.; Liu, H.T. Sedimentary exhalative origin of the Baiyinnuoer zinc-lead deposit, Chifeng, Inner Mongolia: Geological and sulfur isotope evidence. *J. Jilin Univ. (Earth Sci. Ed.)* **2007**, *37*, 659–670. (In Chinese)
- Zeng, Q.; Liu, J.; Zhang, Z.; Jia, C.; Yu, C.; Ye, J.; Liu, H. Geology and lead-isotope study of the Baiyinnuoer Zn–Pb–Ag deposit, South Segment of the Da Hinggan Mountains, Northeastern China. *Resour. Geol.* **2009**, *59*, 170–180. [[CrossRef](#)]
- Xiao, W.J.; Windley, B.F.; Huang, B.C.; Han, C.M.; Yuan, C.; Chen, H.L.; Sun, M.; Sun, S.; Li, J.L. End-Permian to mid-Triassic termination of the accretionary processes of the southern Altaids: Implications for the geodynamic evolution, Phanerozoic continental growth, and metallogeny of Central Asia. *Acta Diabetol.* **2009**, *98*, 1189–1217.
- Zhang, J.-H.; Gao, S.; Ge, W.-C.; Wu, F.-Y.; Yang, J.-H.; Wilde, S.A.; Li, M. Geochronology of the Mesozoic volcanic rocks in the Great Xing’an Range, northeastern China: Implications for subduction-induced delamination. *Chem. Geol.* **2010**, *276*, 144–165. [[CrossRef](#)]
- Zhou, J.-B.; Wilde, S.A. The crustal accretion history and tectonic evolution of the NE China segment of the Central Asian Orogenic Belt. *Gondwana Res.* **2013**, *23*, 1365–1377. [[CrossRef](#)]
- Chen, Y.Q.; Li, C.S.; Zong, D.K. Mineral exploration type and productive exploration in Baiyinnuoer lead-zinc mine. *Nonferrous Mines* **2002**, *31*, 16–18. (In Chinese)
- Jiang, S.-H.; Chen, C.-L.; Bagas, L.; Liu, Y.; Han, N.; Kang, H.; Wang, Z.-H. Two mineralization events in the Baiyinnuoer Zn–Pb deposit in Inner Mongolia, China: Evidence from field observations, S–Pb isotopic compositions and U–Pb zircon ages. *J. Asian Earth Sci.* **2017**, *144*, 339–367. [[CrossRef](#)]
- Wan, Z.M.; Lan, R.W.; Yu, F. Law of alteration zoning, metallic zoning and discussion of production exploration in Baiyinnuoer Pb–Zn deposit, Chifeng. *Miner. Deposits* **2002**, *21*, 467–469. (In Chinese)
- Jiang, S.H.; Nie, F.J.; Bai, D.M.; Niu, S.Y.; Wang, B.D.; Liu, Y.F.; Liu, Y. Study on the lead isotopic features of the Baiyinnuoer Pb–Zn deposit in Inner Mongolia. *J. Earth Sci. Environ.* **2011**, *33*, 230–238. (In Chinese)

16. Yi, J.; Wei, J.H.; Yao, C.L.; Zhao, S.Q.; Yu, C.L.; Li, Q.Y. Discovery and geological significance of the Triassic intrusive rocks in the Baiyinnuoer lead-zinc deposit, Inner Mongolia: Evidence from zircon U–Pb age. *Geol. Sci. Technol. Inf.* **2012**, *31*, 11–16. (In Chinese)
17. Yang, F.; Wang, Y.; Na, F.C.; Fu, J.H.; Zhang, G.Y.; Sun, W.; Pang, X.J.; Chen, J.S.; Liu, M.; Li, B. Geological significance and metallogenic epoch of the Baiyinnuoer Pb–Zn deposit in Inner Mongolia: Constraints from geochemistry and chronology of intrusive rocks. *J. Jilin Univ. (Earth Sci. Ed.)* **2018**, *48*, 1696–1710. (In Chinese)
18. Jahn, B.-M.; Wu, F.; Chen, B. Granitoids of the Central Asian Orogenic Belt and continental growth in the Phanerozoic. In Proceedings of the Fourth Hutton Symposium on the Origin of Granites and Related Rocks, Clermont-Ferrand, France, 20–25 September 2000; Volume 350, pp. 181–193.
19. Jahn, B.M.; Capdevila, R.; Liu, D.; Vernov, A.; Badarch, G. Sources of Phanerozoic granitoids in the transect Bayanhongor–Ulan Baator, Mongolia: Geochemical and Nd isotopic evidence, and implications of Phanerozoic crustal growth. *J. Asian Earth Sci.* **2004**, *23*, 211–219. [[CrossRef](#)]
20. Windley, B.F.; Alexeiev, D.; Xiao, W.J.; Kroner, A.; Badarch, G. Tectonic models for accretion of the Central Asian Orogenic Belt. *J. Geol. Soc. Lond.* **2007**, *164*, 31–47. [[CrossRef](#)]
21. Xiao, W.; Sun, M.; Santosh, M. Continental reconstruction and metallogeny of the Circum-Junggar areas and termination of the southern Central Asian Orogenic Belt. *Geosci. Front.* **2015**, *6*, 137–140. [[CrossRef](#)]
22. Xu, B.; Zhao, P.; Wang, Y.Y.; Liao, W.; Luo, Z.W.; Bao, Q.Z.; Zhou, Y.H. The pre-Devonian tectonic framework of Xing’an-Mongolia orogenic belt (XMOB) in North China. *J. Asian Earth Sci.* **2015**, *97*, 183–196. [[CrossRef](#)]
23. Qi, J.P.; Chen, Y.J.; Pirajno, F. Geological characteristics and tectonic setting of the epithermal deposits in the Northeast China. *J. Mineral. Petrol.* **2005**, *25*, 47–59. (In Chinese)
24. Li, J.-Y. Permian geodynamic setting of Northeast China and adjacent regions: Closure of the Paleo-Asian Ocean and subduction of the Paleo-Pacific Plate. *J. Asian Earth Sci.* **2006**, *26*, 207–224. [[CrossRef](#)]
25. Chen, Y.-J.; Zhang, C.; Wang, P.; Pirajno, F.; Li, N. The Mo deposits of Northeast China: A powerful indicator of tectonic settings and associated evolutionary trends. *Ore Geol. Rev.* **2017**, *81*, 602–640. [[CrossRef](#)]
26. Chen, Y.J.; Zhai, M.G.; Jiang, S.Y. Significant achievements and open issues in study of orogenesis and metallogenesis surrounding the North China continent. *Acta Petrol.* **2009**, *25*, 2695–2726. (In Chinese)
27. Ouyang, H.; Mao, J.; Zhou, Z.; Su, H. Late Mesozoic metallogeny and intracontinental magmatism, southern Great Xing’an Range, northeastern China. *Gondwana Res.* **2015**, *27*, 1153–1172. [[CrossRef](#)]
28. Zhao, Y.M.; Zhang, D.Q. *Metallogeny and Prospective Evaluation of Copper-Polymetallic Deposits in the Da Hinggan Mountains and Its Adjacent Regions*; Seismological Press: Beijing, China, 1997; p. 318. (In Chinese)
29. Niu, S.Y.; Sun, A.Q.; Guo, L.J.; Wang, B.D.; Hu, H.B.; Jian, M. Ore-control structures and prospecting for the Baiyinnuoer Pb–Zn deposit in the Da Hinggan range. *Geotecton. Metallog.* **2008**, *32*, 72–80. (In Chinese)
30. Wang, X.; Xu, D.; Lv, X.; Wei, W.; Mei, W.; Fan, X.; Sun, B. Origin of the Haobugao skarn Fe–Zn polymetallic deposit, Southern Great xing’an range, NE China: Geochronological, geochemical, and Sr–Nd–Pb isotopic constraints. *Ore Geol. Rev.* **2018**, *94*, 58–72. [[CrossRef](#)]
31. Zhai, D.; Williams-Jones, A.E.; Liu, J.; Selby, D.; Li, C.; Huang, X.-W.; Qi, L.; Guo, D. Evaluating the use of the molybdenite Re–Os chronometer in dating gold mineralization: Evidence from the Haigou Deposit, Northeastern China. *Econ. Geol.* **2019**, *114*, 897–915. [[CrossRef](#)]
32. Chen, B.; Jahn, B. Geochemical and isotopic studies of the sedimentary and granitic rocks of the Altai Orogen of NW China and their tectonic implications. *Geol. Mag.* **2001**, *139*, 1–13. [[CrossRef](#)]
33. Li, W.; Zhong, R.; Xu, C.; Song, B.; Qu, W. U–Pb and Re–Os geochronology of the Bainaimiao Cu–Mo–Au deposit, on the northern margin of the North China Craton, Central Asia Orogenic Belt: Implications for ore genesis and geodynamic setting. *Ore Geol. Rev.* **2012**, *48*, 139–150. [[CrossRef](#)]
34. Wang, F.; Zhou, X.-H.; Zhang, L.-C.; Ying, J.-F.; Zhang, Y.-T.; Wu, F.-Y.; Zhu, R.-X. Late Mesozoic volcanism in the Great Xing’an Range (NE China): Timing and implications for the dynamic setting of NE Asia. *Earth Planet. Sci. Lett.* **2006**, *251*, 179–198. [[CrossRef](#)]
35. Wei, C.-S.; Zhao, Z.-F.; Spicuzza, M.J. Zircon oxygen isotopic constraint on the sources of late Mesozoic A-type granites in eastern China. *Chem. Geol.* **2008**, *250*, 1–15. [[CrossRef](#)]
36. Wang, S.M.; Yan, M.H. GB/T 14506.28-2010. *Methods for Chemical Analysis of Silicate Rocks-PART 28: Determination of 16 Major and Minor Elements Content*; Standards Press of China: Beijing, China, 2010. (In Chinese)

37. Ludwig, K.R. *ISOPLLOT 3.00: A Geochronological Toolkit for Microsoft Excel*; Special Publication No. 4; Berkeley Geochronology Center: Berkeley, CA, USA, 2003.
38. Middlemost, E.A.K. *Magma and Magmatic Rocks*; Longman: London, UK, 1985; p. 266.
39. Bas, M.J.L.; Maitre, R.W.L.; Streckeisen, A.; Zanettin, B. A chemical classification of volcanic rocks based on the total alkali-silica diagram. *J. Pet.* **1986**, *27*, 745–750. [[CrossRef](#)]
40. Maniar, P.D.; Piccoli, P.M. Tectonic discrimination of granitoids. *GSA Bull.* **1989**, *101*, 635–643. [[CrossRef](#)]
41. Sun, S.-S.; McDonough, W.F. Chemical and isotopic systematics of oceanic basalts: Implications for mantle composition and processes. In *Magmatism in the Ocean Basins*, 42; Saunders, A.D., Norry, M.J., Eds.; Special Publications; Geological Society: London, UK, 1989; pp. 313–345.
42. Wu, F.-Y.; Jahn, B.M.; Wilde, S.A.; Lo, C.H.; Yui, T.F.; Lin, Q.; Ge, W.C.; Sun, D.Y. Highly fractionated I-type granites in NE China (II): Isotopic geochemistry and implications for crustal growth in the Phanerozoic. *Lithos* **2003**, *67*, 191–204. [[CrossRef](#)]
43. Zartman, R.E.; Doe, B.R. Plumbotectonics: The model. *Tectonophysics* **1981**, *75*, 135–162. [[CrossRef](#)]
44. Hoskin, P.W.; Ireland, T.R. Rare earth element chemistry of zircon and its use as a provenance indicator. *Geol.* **2000**, *28*, 627. [[CrossRef](#)]
45. Guo, Z.J.; Zhou, Z.H.; Li, G.T.; Li, J.W.; Wu, X.L.; Ou, Y.H.G.; Wang, A.S.; Xiang, A.P.; Dong, X.Z. SHRIMP U–Pb zircon dating and petrogeochemical characteristics of the intermediate-acid intrusive rocks in the Aoergai copper deposit of Inner Mongolia. *Geol. China* **2012**, *6*, 1486–1500. (In Chinese)
46. Kang, Y.; She, H.; Lai, Y.; Wang, Z.; Li, J.; Zhang, Z.; Xiang, A.; Jiang, Z. Evolution of Middle-Late Triassic granitic intrusions from the Badaguan Cu–Mo deposit, Inner Mongolia: Constraints from zircon U–Pb dating, geochemistry and Hf isotopes. *Ore Geol. Rev.* **2018**, *95*, 195–215. [[CrossRef](#)]
47. Barbarin, B. A review of the relationships between granitoid types, their origins and their geodynamic environments. *Lithos* **1999**, *46*, 605–626. [[CrossRef](#)]
48. Chappell, B.W.; White, A.J.R. Two contrasting granite types. *Pac. Geol.* **1974**, *8*, 173–174.
49. Loiselle, M.C.; Wones, D.R. Characteristics of anorogenic granites. *Geol. Soc. Am. Abstr. Programs* **1979**, *11*, 468.
50. Chappell, B.W.; White, A.J.R. Two contrasting granite types: 25 years later. *Aust. J. Earth Sci.* **2001**, *48*, 489–499. [[CrossRef](#)]
51. Whalen, J.B.; Currie, K.L.; Chappell, B.W. A-type granites: Geochemical characteristics, discrimination and petrogenesis. *Contrib. Miner. Pet.* **1987**, *95*, 407–419. [[CrossRef](#)]
52. Chappell, B.W.; White, A.J.R. I- and S-type granites in the Lachlan Fold Belt. *Trans. R. Soc. Edinb. Earth Sci.* **1992**, *272*, 1–26.
53. Chappell, B. Aluminium saturation in I- and S-type granites and the characterization of fractionated haplogranites. *Lithos* **1999**, *46*, 535–551. [[CrossRef](#)]
54. Douce, A.E.P.; Harris, N. Experimental Constraints on Himalayan Anatexis. *J. Pet.* **1998**, *39*, 689–710. [[CrossRef](#)]
55. Barbarin, B. Mafic magmatic enclaves and mafic rocks associated with some granitoids of the central Sierra Nevada batholith, California: Nature, origin, and relations with the hosts. *Lithos* **2005**, *80*, 155–177. [[CrossRef](#)]
56. Grove, T.L.; Elkins-Tanton, L.T.; Parman, S.W.; Chatterjee, N.; Gaetani, G.A. Fractional crystallization and mantle-melting controls on calc-alkaline differentiation trends. *Contrib. Miner. Pet.* **2003**, *145*, 515–533. [[CrossRef](#)]
57. Jagoutz, O.; Schmidt, M. The formation and bulk composition of modern juvenile continental crust: The Kohistan arc. *Chem. Geol.* **2012**, *298*, 79–96. [[CrossRef](#)]
58. Rapp, R.; Shimizu, N.; Norman, M.; Applegate, G. Reaction between slab-derived melts and peridotite in the mantle wedge: Experimental constraints at 3.8 GPa. *Chem. Geol.* **1999**, *160*, 335–356. [[CrossRef](#)]
59. Martin, H.; Smithies, R.H.; Moyen, J.F.; Champion, D. An overview of adakite, tonalite–trondhjemite–granodiorite (TTG), and sanukitoid: Relationships and some implications for crust evolution. *Lithos* **2005**, *79*, 1–24. [[CrossRef](#)]
60. Petford, N.; Atherton, M. Na-rich Partial Melts from Newly Underplated Basaltic Crust: The Cordillera Blanca Batholith, Peru. *J. Pet.* **1996**, *37*, 1491–1521. [[CrossRef](#)]
61. Taylor, S.R.; McLennan, S.M. *The Continental Crust: Its Composition and Evolution*; Blackwell: Oxford, UK, 1985.

62. Ersoy, Y.; Helvacı, C. FC-AFC-FCA and mixing modeler: A Microsoft Excel(c) spreadsheet program for modeling geochemical differentiation of magma by crystal fractionation, crustal assimilation and mixing. *Comput. Geosci.* **2010**, *36*, 383–390. [[CrossRef](#)]
63. Wang, W.; Liu, S.; Santosh, M.; Wang, G.; Bai, X.; Guo, R. Neoproterozoic intra-oceanic arc system in the Western Liaoning Province: Implications for Early Precambrian crustal evolution in the Eastern Block of the North China Craton. *Earth Sci. Rev.* **2015**, *150*, 329–364. [[CrossRef](#)]
64. Khain, E.; Bibikova, E.; Kröner, A.; Zhuravlev, D.; Sklyarov, E.; Fedotova, A.; Kravchenko-Berezhnaya, I. The most ancient ophiolite of the Central Asian fold belt: U–Pb and Pb–Pb zircon ages for the Dunzhugur Complex, Eastern Sayan, Siberia, and geodynamic implications. *Earth Planet. Sci. Lett.* **2002**, *199*, 311–325. [[CrossRef](#)]
65. Tang, K. Tectonic development of Paleozoic fold belts at the north margin of the Sino-Korean craton. *Tectonics* **1990**, *9*, 249–260. [[CrossRef](#)]
66. Tang, K.; Yan, Z. Regional metamorphism and tectonic evolution of the Inner Mongolian suture zone. *J. Metamorph. Geol.* **1993**, *11*, 511–522.
67. Shi, Y.; Liu, Z.; Liu, Y.; Shi, S.; Wei, M.; Yang, J.; Gao, T. Late Paleozoic–Early Mesozoic southward subduction-closure of the Paleo-Asian Ocean: Proof from geochemistry and geochronology of Early Permian–Late Triassic felsic intrusive rocks from North Liaoning, NE China. *Lithos* **2019**, *346*, 1–24. [[CrossRef](#)]
68. Liu, Y.; Li, W.; Feng, Z.; Wen, Q.; Neubauer, F.; Liang, C. A review of the Paleozoic tectonics in the eastern part of Central Asian Orogenic Belt. *Gondwana Res.* **2017**, *43*, 123–148. [[CrossRef](#)]
69. Sun, D.-Y.; Gou, J.; Wang, T.-H.; Ren, Y.-S.; Liu, Y.-J.; Guo, H.-Y.; Liu, X.-M.; Hu, Z.-C. Geochronological and geochemical constraints on the Erguna massif basement, NE China—Subduction history of the Mongol–Okhotsk oceanic crust. *Int. Geol. Rev.* **2013**, *55*, 1801–1816. [[CrossRef](#)]
70. Zhang, X.; Yuan, L.; Xue, F.; Yan, X.; Mao, Q. Early Permian A-type granites from central Inner Mongolia, North China: Magmatic tracer of post-collisional tectonics and oceanic crustal recycling. *Gondwana Res.* **2015**, *28*, 311–327. [[CrossRef](#)]
71. Jian, P.; Liu, D.; Kröner, A.; Windley, B.F.; Shi, Y.; Zhang, W.; Zhang, F.; Miao, L.; Zhang, L.; Tomurhuu, D. Evolution of a Permian intraoceanic arc–trench system in the Solonker suture zone, Central Asian Orogenic Belt, China and Mongolia. *Lithos* **2010**, *118*, 169–190. [[CrossRef](#)]
72. Pearce, J.A.; Harris, N.B.W.; Tindle, A.G. Trace Element Discrimination Diagrams for the Tectonic Interpretation of Granitic Rocks. *J. Pet.* **1984**, *25*, 956–983. [[CrossRef](#)]



© 2019 by the authors. Licensee MDPI, Basel, Switzerland. This article is an open access article distributed under the terms and conditions of the Creative Commons Attribution (CC BY) license (<http://creativecommons.org/licenses/by/4.0/>).